ORIGINAL SCIENTIFIC PAPER

CROATICA CHEMICA ACTA

Croat. Chem. Acta **2026**, *99*(2), 137–146
Published online: May 24, 2026
DOI: 10.5562/cca4194

HKD 1926

Mechanical Activation of Carboreduction Pathways in MoO_3 Powders

Nadjia Hammoutene,[1,2] Boualem Bourahla[1,*]

[1] Faculty of Science, M. Mammeri University, BP 17 RP, 15000 Tizi-Ouzou, Algeria
[2] Department of Chemistry, M. Mammeri University, BP 17 RP, 15000 Tizi-Ouzou, Algeria
* Corresponding author's e-mail address: boualem.bourahla@ummto.dz

RECEIVED: August 06, 2025 * REVISED: January 29, 2026 * ACCEPTED: January 29, 2026

Abstract: We explore the mechanism of carbothermic reduction in MoO_3 powders mechanically activated by carbon black. Given the complexity of this system, which involves a mixture of stable and metastable species and complex in situ processes, we combine theoretical and experimental approaches for comprehensive analysis. Ellingham diagrams are used to predict the feasibility of the reaction at different temperatures, whereas the volatility diagrams of the Mo/O/C system are developed to define the conditions under which the solid and gas phases coexist. A mechanically activated mixture of MoO_3 and carbon black, ground for 20 hours, was examined by DSC, TG and DTA analyses at several different temperatures. The resulting solid and gaseous products are characterized via the usual techniques. The obtained results prove that all reactions are more complex when stoichiometric calculations are performed. Moreover, by examining the results of experiments carried out under an argon atmosphere at high temperature, we can identify five main stages in the carbothermic reaction of the mixture MoO_3–C.

Keywords: molybdenum trioxide, molybdenum carbide, carbothermal reaction, ellingham diagram and volatility diagram.

INTRODUCTION

TRANSITION metal carbides are essential materials in modern technology because of their exceptional properties which are comparable to those of noble metals.[1–2] Molybdenum carbide (Mo_2C) is a prominent type of Group VI_B transition metal. In particular, it has excellent catalytic performance in reactions such as water-gas shift (WGS), methane reforming,[3] hydrocarbon isomerization and hydro-treating processes such as hydride sulfurization and hydride nitrogenation.[4–5] Compared with noble metals, the latter offer cost advantages and superior CO poisoning resistance, with a lower CO desorption temperature than platinum group metals.[6]

Traditional synthesis methods for Mo_2C, typically involving high-temperature powder metallurgy (above 1500 K) under vacuum or argon atmospheres,[7] face challenges related to product purity and surface area.[8] Despite advancements, the carbothermal reduction of metal oxides remains the most widely used industrial process.[9] As noted by W. Weimer,[10] while temperature and pressure are critical their size, porosity and impurities play significant roles. W. Gruner's experimental approach,[11] has advanced the study of carbothermal reactions, shedding light on reduction mechanisms and key operational parameters. In addition, the Mo/O/C system is complex and involves stable and metastable phases during thermal processing. Although the characteristics of oxides in the Mo/O system are relatively well understood,[12] a detailed understanding of the reduction mechanism from MoO_3 to metallic carbide is lacking. Saghafi et al.[13] synthesized nanocrystalline molybdenum from MoO_3 via carbon through high-energy milling and thermal treatment and observed intermediate phases of MoO_2 and Mo_2C. H.-Y. Zhu et al.[14] explored MoO_3 sublimation and identified two distinct reaction stages affecting Mo_2C formation. S. Khabbaz et al.[15] investigated the impact of experimental parameters on Mo_2C synthesis, noting the initial formation of a molybdenum intermediate phase. K. Sheybani et al.[16] examined the effects of mechanical activation and microwave heating on reduction efficiency, whereas S. Chaudhury et al.[17] and Bolitschek et al.[18] revealed the

This work is licensed under a Creative Commons Attribution 4.0 International License.

kinetic steps leading to Mo_2C formation and emphasized the importance of molar ratios in production of high-purity molybdenum carbide.

Our objective in the present work is to elucidate the solid-phase reaction dynamics and mechanisms of carbothermal reduction for a mixture of mechanically activated MoO_3 and carbon black where the reaction is as follows: $2MoO_3(s) + 7C(s) \rightarrow Mo_2C(s) + 6CO(g)$. The mixture was milled for 20 hours and analyzed within a temperature range of up to 850 °C under an argon atmosphere. The overall structure of the paper is outlined as follows. In next Section, we address the thermodynamic analysis of Mo and its two oxides as a function of temperature at atmospheric pressure of carbon monoxide. In Section 3, we illustrate our experimental procedure to sample the MoO_3–C mixture under thermal treatment at various temperatures. In Section 4, we report and discuss the results of the MoO_3–C powder mixtures by analyzing the morphology and several phases of the MoO_3–C mixture. Conclusions follow in last Section.

THERMODYNAMIC STUDIES

Ellingham Diagram

The Ellingham diagram in Figure 1 is constructed using data sourced from JANAF tables.[19]

This diagram outlines the stability domains of Mo(s), MoO_2(s) and MoO_3(s) as a function of temperature under 1 atm of CO. Three theoretical transition temperatures are identified, the C/CO_2-Mo/MoO_3 intersection at 600 K (327 °C), the C/CO-Mo/MoO_3 intersection at 790 K (517 °C), and the C/CO-Mo/MoO_2 intersection at 1020 K (747 °C). The diagram also shows the intersection of the C/CO and C/CO_2 lines at approximately 980 K (707 °C).

Volatility Diagrams

The diagram, in Figure 2a, represents the existence domain of the Mo_2C carbide and phases of the Mo/O system. At T = 700 K, the carbide stabilizes at $p_{CO} = 10^{-1.8585}$ Pa and $p_{O2}=10^{-27.179}$ Pa. The diagram shows two possible pathways for the conversion of oxides to carbides.

Pathway 1: involves the formation of species $MoO_3(s) \rightarrow MoO_2(s) \rightarrow Mo(s) \rightarrow Mo_2C(s)$.

Pathway 2: involves the species $MoO_3(g)$ in the gaseous state.

As the temperature increases, the stability domains of both molybdenum carbide and its oxides shift toward higher partial pressures of O_2 and CO. This trend is illustrated in Figure 2b for temperatures of 800 K, 900 K, and 1000 K, indicating enhanced thermodynamic stability of these phases at elevated temperatures.

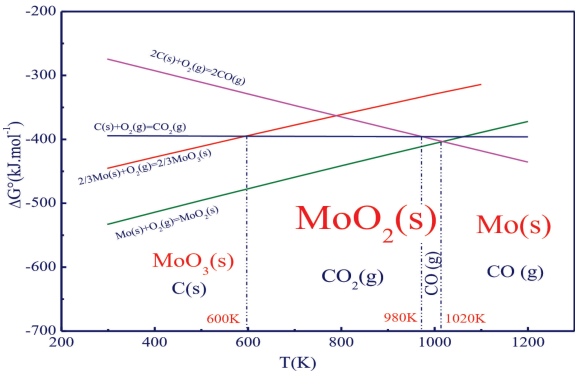


Figure 1. Ellingham diagram of the Mo/O/C system.

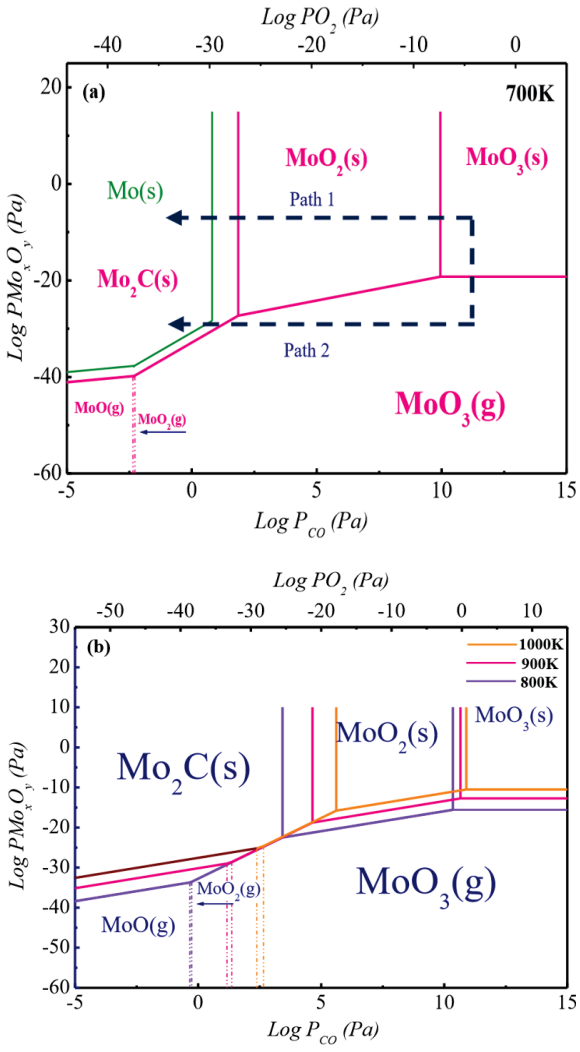


Figure 2. Volatility diagram of the Mo/O/C system, as a function of the CO and O_2 partial pressures: (a) at 700 K, (b) at 800 K, 900 K and 1000 K.

MATERIALS AND EXPERIMENTAL PROCEDURES

Raw Materials

The molybdenum trioxide powder used crystallizes in the orthorhombic system, as evidenced by the X-ray diffraction (XRD) pattern in Figure 3, indexed with card PDF-2 No. 00-0050506.

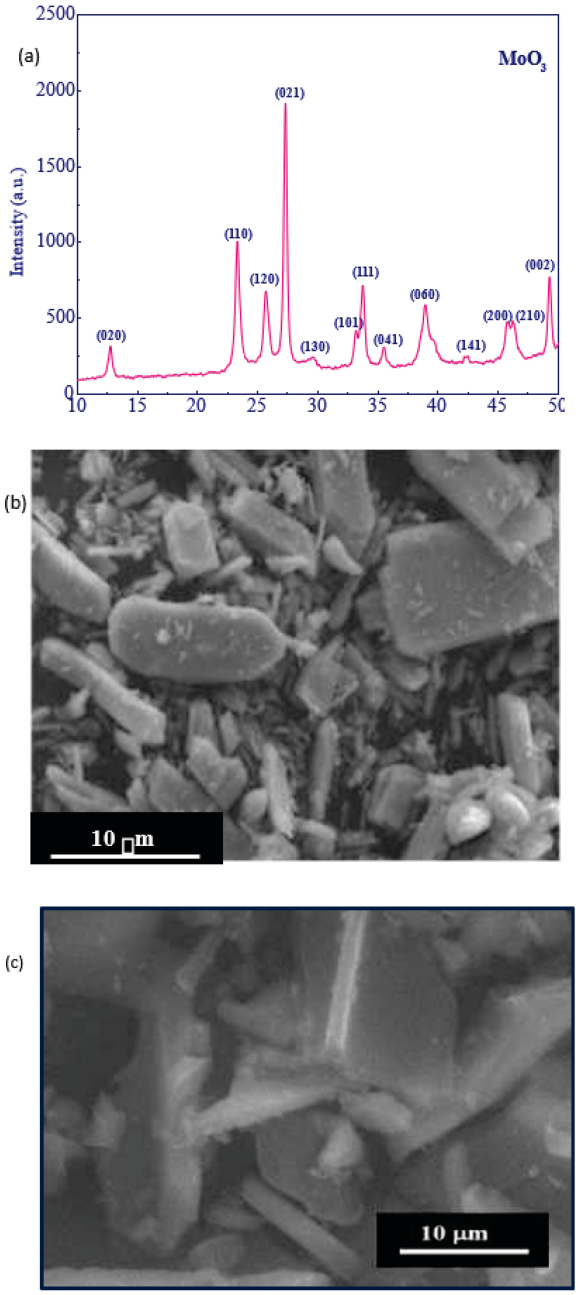


Figure 3. (a) XRD pattern of MoO_3 powder, (b) SEM image of MoO_3 powder, (c) SEM image of the carbon black powder.

Preparation and Pre-Heating Characterization of the MoO_3–C Mixture

Before the heat treatments aimed at studying the carboreduction of MoO_3, the MoO_3–C mixture was prepared to ensure intimate contact and optimal homogeneity. MoO_3 and carbon black were weighed according to a 2 : 7 stoichiometric ratio (MoO_3 : C) and initially mixed in 15 g batches in an agate mortar. The powders were then dried at 100 °C to remove residual surface moisture.

Milling Procedure

The mixture was milled for 20 hours in a 50 cm^3 agate jar using a SPEX 8000M® 3D energy mill containing two agate beads (d_1 = 11.30 mm, m_1 = 1.60897 g; d_2 = 7.25 mm, m_2 = 0.42764 g) with a constant beads-to-powder mass ratio of 2 / 15. The mill operates using high-frequency vibrations (~20 Hz, 1200 rpm) in three orthogonal directions, ensuring continuous and intensive milling.

A milling duration of 20 hours was chosen to achieve substantial particle size reduction, a highly homogeneous mixture, and maximal contact between MoO_3 and carbon. According to the literature,[20–21] shorter milling times (e.g. 5 hours) only slightly broaden XRD peaks without inducing phase changes, whereas extended milling partially amorphizes graphite, introduces structural defects, and significantly enhances reactivity.

Pre-Heating Characterization of the MoO_3–C Mixture

In the present work, the milling was carried out using a SPEX 8000M Mill (≈ 1200 rpm), whose milling energy is significantly higher than that of a planetary mill. Our analyses indicate that duration of 20 hours is sufficient to obtain a homogeneous and reactive mixture. In Figure 4, SEM analysis highlights the impact of milling on particle morphology.

The non-milled mixture (Figure 4a) displays prismatic MoO_3 crystals surrounded by dark amorphous carbon agglomerates, indicating limited contact between the phases. After 20 hours of milling (Figure 4b), the prismatic crystals disappear, replaced by fractured and deformed particles agglomerated at the submicron scale, forming a highly homogeneous mixture. These experimental results confirm that 20 hours represents an optimal compromise, sufficient to mechanically activate the mixture without causing excessive agglomeration or contamination.

Heat Treatment

Samples of 0.25 g of the MoO_3-C mixture, ground for 20 hours, were accurately weighed and placed in a 2.75242 g platinum crucible using a Sartorius3 analytical balance. Before heating, a half-hour vacuum was applied, followed by purging with argon at 18 L min^{-1} to desorb the

adsorbed gases. The furnace was heated to the desired temperature at a rate of 10 °C min^{-1} and the crucible was placed in the hot zone once stabilized.

Thermal treatments were systematically applied at 350 °C (2 h), 500 °C (10 min), 550 °C (10 min), 700 °C (10 min), 750 °C (10 min), 800 °C (10 min), and 850 °C (2 h). Short dwell times were intentionally chosen to isolate the onset and initial progression of the thermochemical reactions identified by TG / DTG analyses, while extended treatments at 350 °C and 850 °C were implemented to ensure advanced reaction completion, thereby enabling robust phase evolution analysis and gas-phase characterization.

Characterization of Solid-State Species

The solid species were characterized by X-ray diffraction (XRD) using a Bruker D8-Advance diffractometer with a Cu anode source, over a 2θ range of 10°–60°, with 0.02° step size and 1 s acquisition time per step. The specific surface areas of the initial powders were determined by the BET method using N_2 physisorption at –196 °C, after vacuum degassing at 300 °C for 6 hours. The morphology of MoO_3 and the resulting carbides was studied by high-resolution ESEM coupled with EDS-X analysisat20 kV.

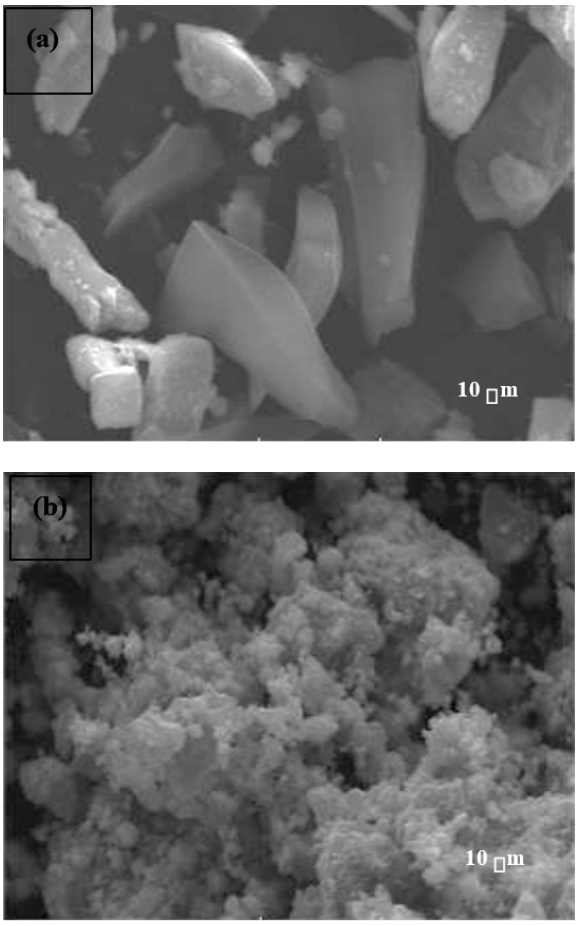


Figure 4. (a) SEM image of the unmilled MoO_3–C mixture, and (b) SEM image of the MoO_3–C mixture after 20 hours of milling.

RESULTS AND DISCUSSIONS

Morphological Observations: EDX Analysis

EDX analyses, the results of which are presented in Figure 5, reveal a significant proportion of nanometric particles. With the exception of a few carbon agglomerates, the particle distribution is homogeneous.

The microstructure, resulting from prolonged grinding, suggests close contact between MoO_3 and carbon black, conducive to the activation of reduction reactions.

Phase Analysis Before Heat Treatment

XRD AND SEM ANALYSIS BEFORE HEAT TREATMENT

Figure 6 shows the XRD spectrum (JCP-2: 00-005-0508), related to the SEM image of the mixture ground for 20 hours (Figure 5). The analysis reveals a remarkable

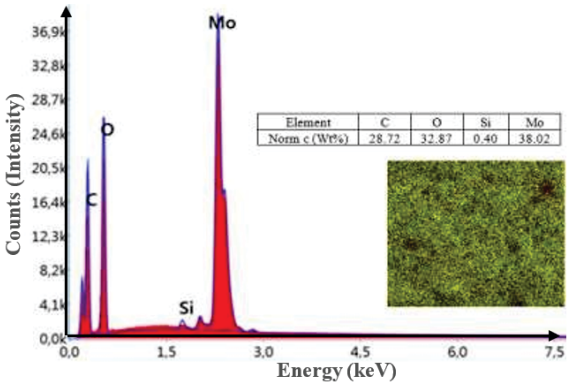


Figure 5. EDX image of MoO_3–C mixed and milled for 20 hours. Its SEM image is shown inside.

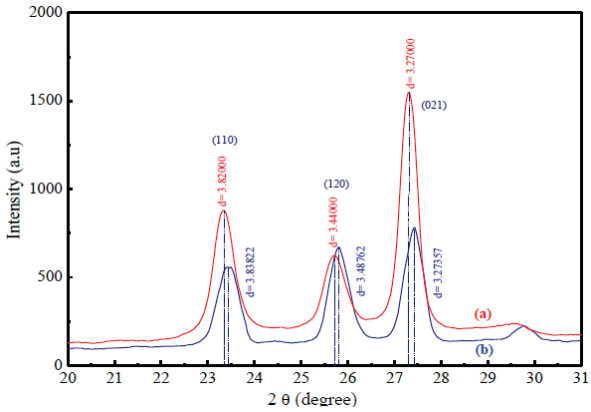


Figure 6. XRD diagrams: (a) of the unground mixture, (b) of the mixture ground for 20 hours, (before heat treatment).

homogeneity of the material, reflecting a uniform distribution of phases. In addition, prolonged grinding enables a nanometric grain size to be achieved, giving the mixture significantly improved reactivity for both solid/solid and solid/gas reactions.

DTA ANALYSIS

The DTA thermogram of the MoO_3-C mixture ground for 20 hours (Figure 7) shows six exothermic peaks at temperatures of 360, 500, 800 and 830 °C. Among these temperatures, three (360, 500 and 800 °C) are close to the theoretical values predicted by the Ellingham lines.

TG/DTG ANALYSIS

Figure 8 presents the TG/DTG analysis which reveals seven successive mass losses, indicating a complex thermal evolution of the mixture. An initial desorption is observed below 150 °C, followed by several minima on the DTG curve around 350 °C, 500 °C, 550 °C, 750 °C, 800 °C and 850 °C, reflecting different stages of thermal transformation.

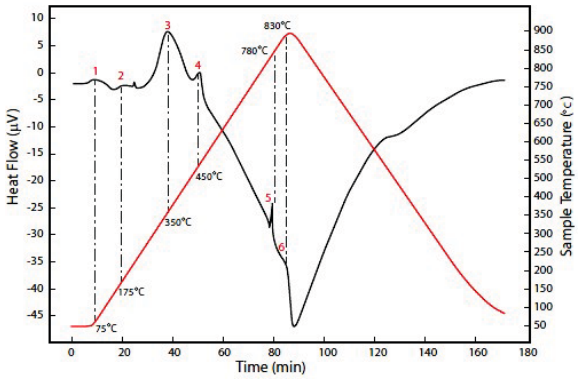


Figure 7. Thermogram DTA of the MoO_3–C mixture ground for 20 hours.

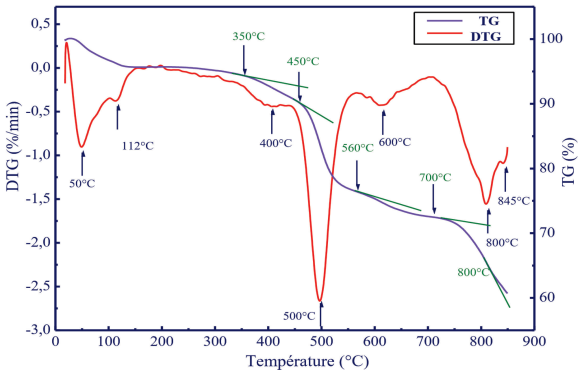


Figure 8. TG and DTG thermograms of the MoO_3–C mixture ground for 20 hours.

To elucidate the reactions responsible for the observed mass losses, isothermal treatments were conducted at 350 °C, 500 °C, 550 °C, 800 °C and 850 °C, selected based on significant variations in the TG curve. Additional experiments were performed in a furnace coupled with a gas chromatograph-mass spectrometer (GC-MS) lasting 2 hours, aiming to identify the gases potentially released (O_2, CO, CO_2).

Phase Analysis Via XRD After Heat Treatment

PHASE ANALYSIS AT 350°C

Figure 9 shows the X-ray diffractogram of the MoO_3–C mixture after heat treatment at 350°C.

It indicates that the mixture remains composed of MoO_3, consistent with the PDF-2 card (No. 01-089-5108).

Heat treatment at 350 °C leads to an increase in peak intensity and sharpening, reflecting an improvement in MoO_3 crystallinity.

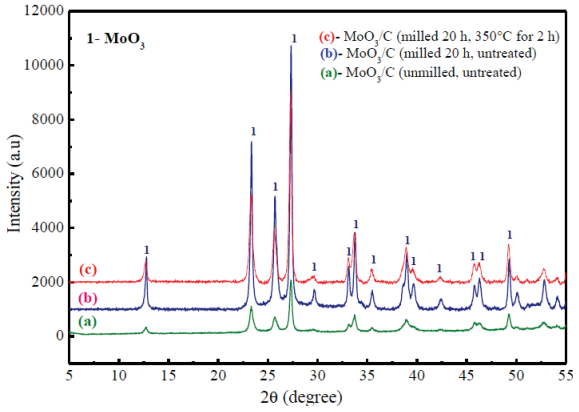


Figure 9. XRD patterns of the MoO_3–C mixture: (a) milled for 20 hours and heat-treated at 350 °C for 2 hours, (b) milled for 20 hours and untreated, and (c) unmilled and untreated.

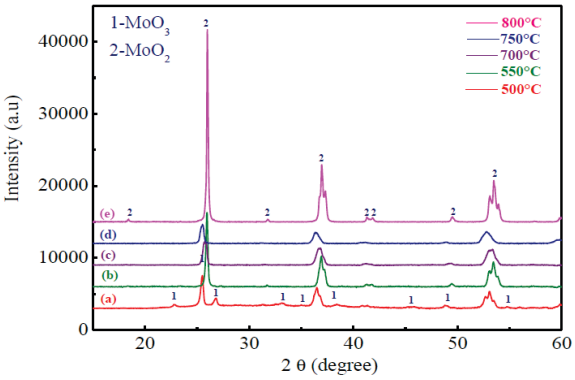


Figure 10. XRD patterns of MoO_3–C mixtures milled for 20 hours and treated at temperature: (a) T = 500 °C, (b) T = 550 °C, (c) T = 700 °C, and (d) T = 800 °C.

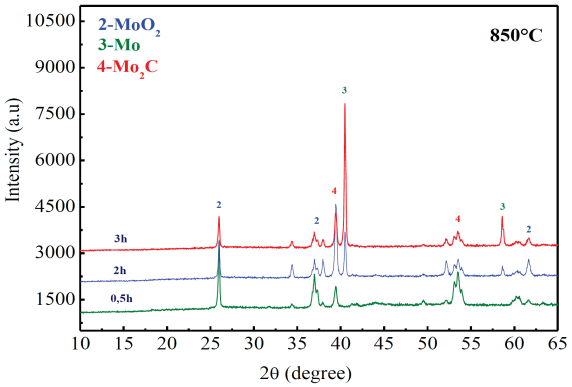


Figure 11. XRD patterns of MoO_3–C mixtures milled for 20 hours and treated at temperature 850 °C, for, respectively, ½, 2 and 3 hours.

PHASE EVOLUTION OF MoO_3–C TOWARD MoO_2: XRD STUDY BETWEEN 500 °C AND 800 °C

The phase evolution of the MoO_3–C mixture between 500 °C and 800 °C was investigated by XRD to track the progressive formation of MoO_2 during the carbothermal reduction process. The results are presented in Figure 10.

XRD ANALYSIS OF THE MoO_3–C MIXTURE POWDER MILLED FOR 20 HOURS AND TREATED AT 850 °C

After thermal treatment at 850 °C, XRD analysis was performed on a MoO_3–C mixture. After 30 min, no trace of molybdenum was detected. The characteristic peaks of MoO_2 remain predominant, with a notable presence of Mo_2C peaks as well. Subsequently, thermal treatments of 2 and 3 hours were conducted to observe the evolution of the different phases at this temperature. The results of these analyses are shown in Figure 11.

XRD analyses reveal the presence of MoO_2, Mo and Mo_2C. An experiment was therefore conducted to verify whether molybdenum carbide can form by interaction between metallic molybdenum and CO released by the MoO_3–C mixture.

The molybdenum powder was then analyzed via EDX, as shown in Figure 12. In this process, CO adsorbs onto the metal, depositing carbon on it while releasing oxygen.[22]

Gas Chromatographic (GC) Analysis of Evolved Gases

Gas chromatographic analyses were systematically performed to identify the gaseous species evolved during the thermal treatment of the MoO_3–C mixture. The gases O_2, CO, and CO_2 were analyzed using a Shimadzu GC-2014 gas chromatograph equipped with a Carbosieve packed column (approximately 3 m in length and 1.6 mm internal diameter), selected for efficient separation of permanent gases. The samples were heated to the target temperature

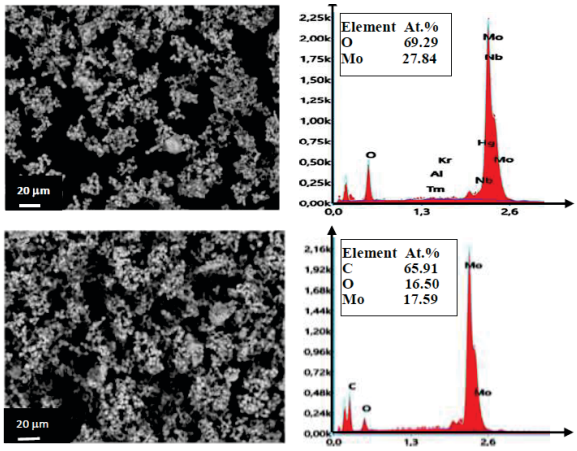


Figure 12. (At the top) EDX image of untreated molybdenum. (At the bottom) EDX image of molybdenum treated at 850 °C.

at a controlled rate of approximately 10 °C min^{-1}, held isothermally for 1 hour, and subsequently purged with high-purity argon (99.995 %) at a flow rate of 1.5 L h^{-1}.

Gas identification was achieved by comparing the retention times with those obtained from certified reference gases. Detection was performed using a thermal conductivity detector (TCD). The chromatographic operating conditions and the corresponding retention times of the detected species are summarized in Table 1.

The gaseous species evolved during the thermal treatment of the MoO_3–C mixture mechanically activated by 20 hours of ball milling were analyzed at selected temperatures to identify the reaction products and to gain mechanistic insight into the decomposition behavior and carbothermal reduction pathways of MoO_3.

EVOLUTION OF CO, CO_2 AND O_2 AT 350 °C

The GC chromatogram of the MoO_3–C mixture (Figure 13a) indicates the evolution of CO and CO_2, with CO being the predominant species, reflecting the onset of carbothermal reactions at this temperature. Notably, no O_2 signal is detected, suggesting rapid consumption of oxygen by carbon or reduced molybdenum species.

In contrast, the GC analysis of pure MoO_3 (Figure 13b) reveals the evolution of O_2, with a retention time of 1.586 min, clearly confirming that oxygen release originates from the thermal decomposition of MoO_3 in the absence of carbon.

Table 1. Gas chromatographic retention times of O_2, CO and CO_2.

Gas	O_2	CO_2	CO
Retention time / min	1.551	15.652	3.081

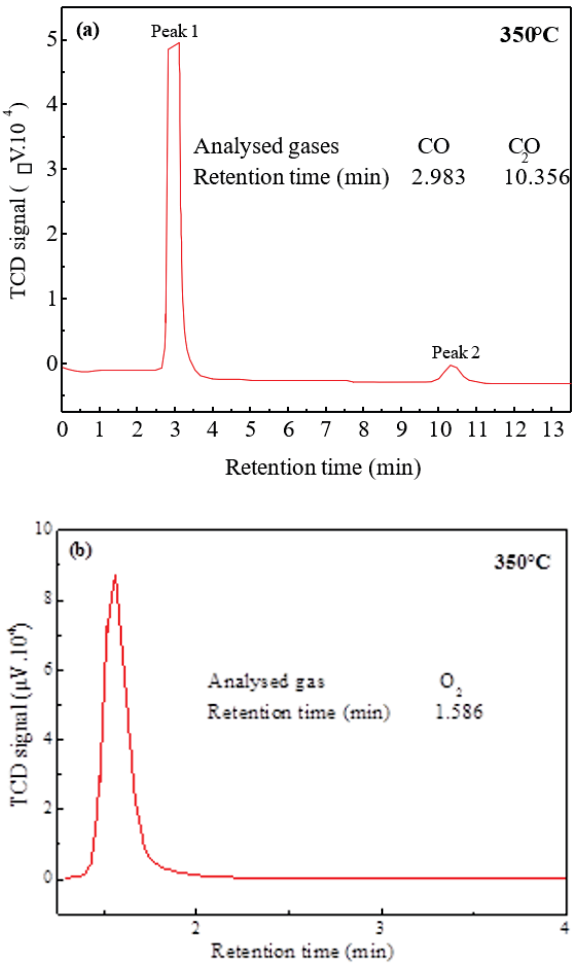


Figure 13. CG chromatograms recorded at 350 °C for: (a) the MoO_3–C mixture, and (b) MoO_3 powder, showing the evolution of CO, CO_2 in the mixture and O_2 from MoO_3.

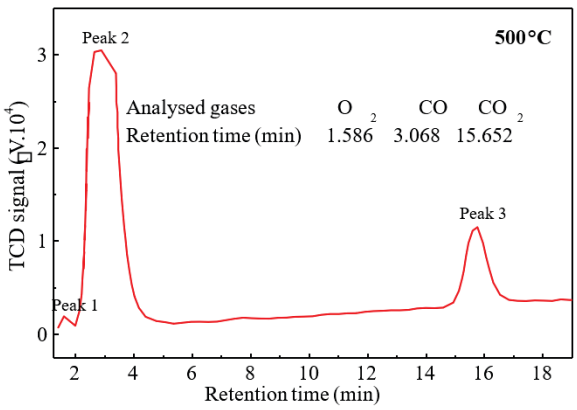


Figure 14. Gas chromatographic (GC) profile of the MoO_3–C mixture obtained at 500 °C, highlighting the evolution of O_2, CO, and CO_2

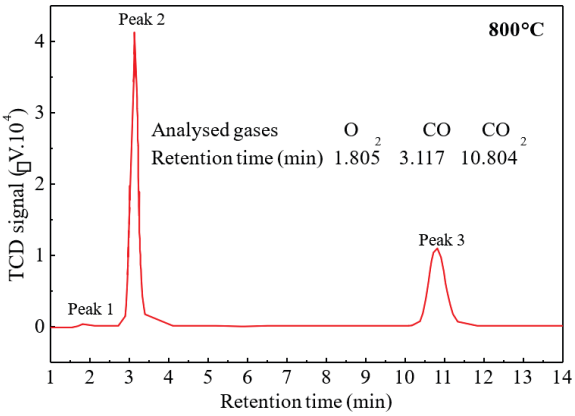


Figure 15. GC chromatogram of the MoO_3–C mixture recorded at 800 °C, showing the evolution of O_2, CO and CO_2.

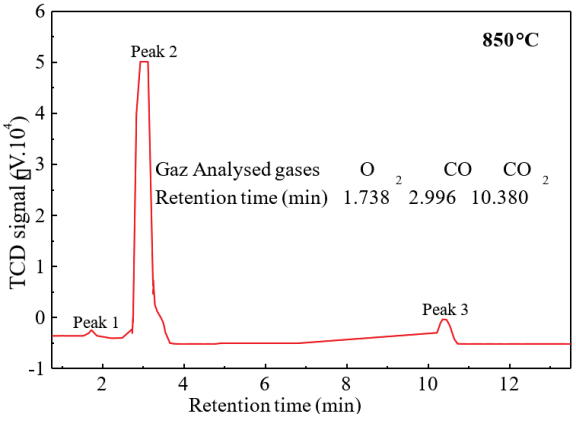


Figure 16. GC chromatogram of the MoO_3–C mixture recorded at 850 °C, showing the evolution of O_2, CO and CO_2.

GAS EVOLUTION AT 500 °C

Thermal treatment at 500 °C was performed using ball-milled MoO_3 (20 hours) and carbon positioned in separate zones of the reactor, with a glass-wool bed acting as a spacer to suppress direct solid–solid contact while permitting gas-phase transport (Figure 14). Following an isothermal dwell of 1 hour, a regulated argon flow was introduced to transfer the evolved gaseous species to the GC analyzer. The resulting chromatogram displays welldefined peaks corresponding to O_2 (1.586 min), CO (3.068 min), and CO_2 (15.652 min). The concurrent detection of oxygen- and carbon-containing species indicates substantial gas evolution and provides compelling evidence for the active progression of carbothermal reduction reactions at this temperature, likely governed by a combination of solid–gas interactions and gas-phase transport processes.

ADVANCED REDUCTION Of MoO_3 AT 800 °C

At 800 °C, the GC chromatogram (Figure 15) displays well-defined peaks corresponding to O_2 (1.805 min), CO (3.117 min), and CO_2 (10.804 min). The pronounced intensities of the CO and CO_2 signals reflect an advanced carbothermal reduction stage, associated with extensive oxidation of carbon and rapid oxygen removal from the oxide lattice. These findings are in excellent agreement with the XRD analysis, which indicates the near-complete consumption of MoO_3 and the formation of reduced molybdenum oxide phases, predominantly MoO_2, confirming the advanced progression of the reduction process at this temperature.

PREDOMINANT FORMATION OF CO AT 850 °C

The MoO_3–C mixture was subjected to thermal treatment at 850 °C under continuous GC monitoring (Figure 16). After an isothermal dwell of 1 hour, a regulated argon flow was introduced to convey the evolved gaseous species to the GC analyzer. The resulting chromatogram exhibits well-resolved peaks corresponding to O_2 (1.738 min), CO (2.996 min), and CO_2 (10.380 min), with CO clearly dominating the gas composition.

The strong predominance of CO reflects an advanced and nearly complete carbothermal reduction regime, characterized by efficient oxygen removal from the molybdenum oxide lattice and extensive oxidation of carbon. This interpretation is in excellent agreement with the XRD results, which demonstrate the near-total disappearance of MoO_3 and its transformation into reduced molybdenum oxide phases, predominantly MoO_2, at this temperature.

DISCUSSION

At 350 °C, the onset of interaction between MoO_3 and carbon becomes clearly discernible. Differential thermal analysis (Figure 7) exhibits a distinct exothermic event (peak No. 3), while the corresponding TG curve (Figure 8) reveals the initiation of mass loss. This mass loss is attributed to the evolution of CO and CO_2, as unequivocally confirmed by the GC chromatogram in Figure 13a.

To decouple the role of carbon, pure MoO_3 powder was subjected to identical thermal conditions. Under these conditions, GC analysis shows the release of O_2, demonstrating that oxygen liberated during the thermal decomposition of MoO_3 is rapidly scavenged in the MoO_3–C mixture, where it reacts with carbon to generate CO and CO_2.

Although the formation of CO at 350 °C is thermodynamically unfavorable according to the Boudouard equilibrium ($C + CO_2 \rightleftharpoons 2\ CO$), which becomes spontaneous only above approximately 700 °C,[23] its early detection indicates that the process is dominated by rapid, kinetically controlled pathways. These pathways are most likely facilitated by the mechanical activation induced by ball milling, which enhances solid–solid contact, increases defect density, and promotes accelerated reaction kinetics at low temperatures.

In addition, solid–solid MoO_3–C reactions may already occur when interparticle contact is sufficient, consistent with the Ellingham diagram, which predicts the reduction of MoO_3 by carbon from 327 °C (600 K), (see Figure 1).

The reactions likely to occur around 350 °C are as follows:

$$MoO_3(s) \rightarrow MoO_{3-x}(s) + \frac{x}{2}O_2(g)$$

$$MoO_3(s) + C(s) \rightarrow MoO_{3-x}(s) + CO(g)\ \text{(dominant)}$$

$$MoO_3(s) + C(s) \rightarrow MoO_{3-x}(s) + CO_2(g)\ \text{(minor)}$$

At 500 °C, GC analysis (Figure 14) evidences the simultaneous evolution of CO, CO_2 and O_2, with CO clearly predominating. The marked increase in gas release relative to 350 °C correlates well with the enhanced mass loss observed in the TG curve, while the associated DTG peak identifies the temperature range of maximum reaction rate. Consistently, XRD analysis of the sample treated for 10 min at 500 °C (Figure 10) reveals the formation of MoO_2 together with residual MoO_3, indicating that the carbothermal reduction remains incomplete at this stage.

At 800 °C, GC analysis (Figure 15) again detects the evolution of CO, CO_2 and O_2, confirming the persistence of the same gas-phase products. Over the temperature interval from 500 to 800 °C, the reduction of MoO_3 proceeds through a continuous and progressive pathway, leading to the gradual conversion of MoO_3 to MoO_2 while releasing a mixed gaseous phase composed of CO, CO_2 and O_2. This evolution is unambiguously supported by the XRD patterns, which demonstrate the progressive disappearance of MoO_3 and the exclusive presence of the MoO_2 phase at 800 °C, as shown in Figure 10. The reactions likely to occur within this temperature range are as follows:

$$MoO_3(s) \rightleftharpoons MoO_2(s) + \frac{1}{2}\ O_2(g)$$

$$C + \frac{1}{2}\ O_2 \rightleftharpoons CO$$

$$MoO_3 + CO \rightleftharpoons MoO_2 + CO_2$$

At 850 °C, GC analysis (Figure 16) reveals the evolution of CO, CO_2 and O_2, with CO overwhelmingly dominating the gas composition, indicating a strongly reducing environment. Thermal analyses confirm that the reaction remains highly

active at this temperature, as evidenced by the pronounced exothermic event (peak No. 6) in the DTA curve (Figure 7) and the corresponding DTG signal near 840 °C (Figure 8). XRD patterns (Figure 11) demonstrate the coexistence of metallic Mo and Mo_2C, reflecting the advanced reduction of molybdenum oxides and the onset of carbide formation.

These experimental observations are in excellent agreement with the volatility diagram at 1100 K (Figure 17), which indicates that Mo and Mo_2C share a common thermodynamic stability domain, as well as with the Ellingham diagrams (Figure 1), which predict that above approximately 747 °C, the thermodynamically stable species in the Mo–O–C system are metallic Mo and CO.

The persistence of a residual fraction of MoO_2 can be attributed to kinetic limitations, as shown by Samsuri et al.[20] and Wang et al.[21] for the reduction of MoO_3 by CO.

The appearance of the carbide at 850 °C raises the question of its formation mechanism. The formation of Mo_2C seems unlikely via a solid–solid reaction between MoO_2 and C, which would require intimate contact that is difficult to maintain after the previous transformations. In contrast, a gas–solid reaction involving CO and Mo appears more plausible:

$$2\ Mo + CO \rightarrow MoO$$

At this temperature, the formation of Mo_2C likely occurs via a gas / solid mechanism rather than a solid/solid reaction with MoO_2. The CO released by the MoO_3–C mixture at 850 °C can adsorb onto metallic Mo and deposit carbon, a mechanism well documented in the literature.[24–26] This hypothesis is confirmed by a complementary test: a Mo sample placed above the mixture and heated for 2 hours at 850 °C shows carbon deposition by EDX images (Figure 12-Top), absent in the control (Figure 12-Bottom). Initially, Mo is mainly O (69.3 at. %) and Mo (27.8 at.%), with minor artifacts (<1.5 at.%). After heating under Ar with MoO_3–C, the surface exceeds 65 at.% C, demonstrating significant carbon deposition under inert conditions.

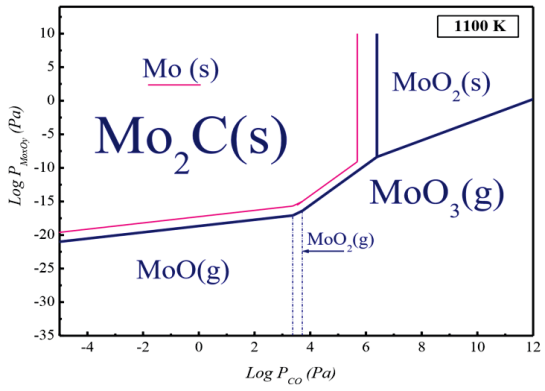


Figure 17. Volatility diagram of the Mo/O/C system as a function of the partial pressure of carbon monoxide at 1100 K.

Although this analysis does not directly identify Mo_2C, XRD performed under the same conditions confirms its formation.

These results are consistent with the work of Rao et al.[27] who demonstrated that Mo reacts with CO to form Mo_2C between 1123 K and 1298 K (≈ 850–1025 °C) with favorable kinetics. Furthermore, studies by Hiraoka et al.[28] and Imai et al.[29] show that carbon can diffuse into Mo at high temperature, allowing carbide formation once the local carbon concentration is sufficient.

Thus, Mo_2C formation at 850 °C most likely follows a two-step mechanism:

- Adsorption and dissociation of CO at the Mo surface, providing active carbon.
- Interstitial diffusion of carbon into Mo, leading to carbide formation.

Overall, experimental observations, thermodynamic predictions, and previous studies converge clearly toward this mechanism.[30]

CONCLUSIONS

Our study presents several original results compared to previous work. In these earlier studies, authors examined the carbothermic reduction of MoO_3 by carbon; among them, we cite Khabbaz et al.[,15] Sheybani et al.,[16] Chaudhury et al.,[17] Chen et al.,[31] Suryananaravana,[32] and Sun et al.[8] Their studies were conducted either under non-isothermal conditions or with short-duration mechanical grinding, sometimes in the presence of additives or under microwave irradiation, and focused mainly on the final formation of Mo or Mo_2C phases, without detailed monitoring of intermediate species or microstructure. Our study differs considerably from the approaches followed by the aforementioned authors. We performed an isothermal study under argon scanning on the mixture (2 MoO_3 + 7 C), both in its unmilled state and after prolonged mechanical milling of 20 hours. The experiments, conducted from 350 °C to 850 °C, made it possible to follow the progressive evolution of the species formed and to highlight the simultaneous coexistence of MoO_2, Mo and Mo_2C, a phenomenon not reported in previous studies. In addition, a thermodynamic study based on Ellingham and volatility diagrams was conducted to identify the theoretical stability ranges of the species likely to form at each temperature, depending on the gaseous composition of the system, and to compare these predictions with experimental observations, thus strengthening the interpretation of the proposed reaction mechanisms.

The originality of the results obtained lies in:

- The unique combination of prolonged mechanical activation and systematic isothermal monitoring under an argon atmosphere;

- The detailed monitoring of the formation and coexistence of the MoO_2, Mo, and Mo_2C phases;
- The rigorous correlation between the experimental results and the thermodynamic calculations.

These elements confirm the originality of our approach, which combines prolonged mechanical activation, detailed isothermal monitoring and thermodynamic predictions of the reaction mechanisms of the MoO_3–C system.

Acknowledgment. The authors are very indebted to N. M., S. S. and S. C. for editing the manuscript.

REFERENCES

[1] T. Moa, J. Xuc, Y. Yanga, Y. Li, *Catal. Today* **2016**, *261*, 101–115. https://doi.org/10.1016/j.cattod.2015.07.014

[2] Z. Lin, S. R. Denny, J. G. Chen, *J. Catal*. **2021,** *404*, 929–642. https://doi.org/10.1016/j.jcat.2021.06.022

[3] N. M. Schweitzer, J. A. Schaidle, O. K. Ezekoye, X. Pan, S. Linic, L. T. Thompson, *J. Am. Chem. Soc.* **2011**, *133*, 2378–2381. https://doi.org/10.1021/ja110705a

[4] N. Czaplika, A. Rogala, I. Wysocka, *Int. J. Mol. Sci.* **2021**, *22*, 12337. https://doi.org/10.3390/ijms222212337

[5] F. Zhou, Y. Zhou, G. G. Liu, C. T., Wang, J. Wang, *Rare Metals* **2021**, *40*, 3375–3405. https://doi.org/10.1007/s12598-021-01735-y

[6] X. Du, R. Zhang, D. Li, C. Hu, H. Garcia, *J. Ener. Chem.* **2022**, *73*, 68–87. https://doi.org/10.1016/j.jechem.2022.05.014

[7] K. M. Reddy, T. N. Rao, J. Revathi, J. Joardar, *J. Alloys Comp*. **2010**, *494*, 386–391. https://doi.org/10.1016/j.jallcom.2010.01.055

[8] G. D. Sun, G. H. Zhang, B. J. Yan, K. C. Chou, *Int. J. Appl. Ceram. Technol.* **2020**, *17*, 917–931. https://doi.org/10.1111/ijac.13473

[9] S. Pak, S. Kim, J. Lim, T. Kim, K. H. Park, S. Cha, *J. Phys. Chem. C* **2023**, *127*, 4689–4695. https://doi.org/10.1021/acs.jpcc.2c07542

[10] A. W. Weimer (ed.), Carbide, Nitride and Boride Materials Synthesis and Processing, Chapman& Hall, 1997. https://doi.org/10.1007/978-94-009-0071-4

[11] W. Gruner, S. Stolle, L. M. Berger, K. Wetzig, *Int. J. Refr. Met. Hard Mat.* **1999**, *17*, 227–234. https://doi.org/10.1016/S0263-4368(98)00071-7

[12] B. Bokhonov, Y. Borisova, M. Korchagin, *Carbon* **2004**, *42*, 2067–2071. https://doi.org/10.1016/j.carbon.2004.04.016

[13] M. Saghafi, A. Ataie, S. Heshmati-Manesh, *Int. J. Refr. Met. Hard Mat.* **2011**, *29*, 419–423. https://doi.org/10.1016/j.ijrmhm.2010.12.012

[14] H. Y. Zhu, Z. B. Li, H. S. Yang, L. G. Luo, *J. Iron Steel Res. Int.* **2013**, *20*, 51–56.

[15] S. Khabbaz, A. Honarbakhsh-Raouf, A. Ataie, M. Saghafi, *Int. J. Refr. Met. Hard Mat.* **2013**, *41*, 402–407. https://doi.org/10.1016/S1006-706X(13)60176-4

[16] K. Sheybani, S. Javadpour, *Int. J. Refr. Met. Hard Mat*. **2020**, *93*, 105269 https://doi.org/10.1016/j.ijrmhm.2020.105269

[17] S. Chaudhury, S. K. Mukerjee, V. N. Vaidya, V. Venugopal, *J. Alloys Comp*. **1997**, *261*, 105–113. https://doi.org/10.1016/S0925-8388(97)00212-0

[18] J. Bolitschek, S. Luidold, M. O'Sullivan, *Inter. J. Refr. Met. Hard Mat.* **2018**, *71*, 325–329. https://doi.org/10.1016/j.ijrmhm.2017.11.037

[19] D. R. Stull, JANAF Thermochemical Tables, Vol 1. Clearinghouse, **1965**.

[20] A. Samsuri, T. Tengku Shafazila, F. Salleh, R. Othaman, M. W. Mohamed Hisham, M. Ambar Yarmo, *Int. J. Hydrogen Energy* **2020**, *46*, 24831–24844. https://doi.org/10.1016/j.ijhydene.2020.08.214

[21] L. Wang, Z. L. Xue, A. Huang, F. F. Wang, *ACS Omega* **2019**, *4*, 20036–20047. https://doi.org/10.1021/acsomega.9b03171

[22] S. Brunauer, P. H. Emmet, E. Teller, *J. Am. Chem. Soc.* **1938**, *60*, 309–319. https://doi.org/10.1021/ja01269a023

[23] D. R. Gaskell, *Introduction to the Thermodynamics of Materials: CD-ROM*, Vol. 2, Taylor & Francis, US, **2008**.

[24] N. V. Petrova, *J. Phys. Chem. Solids* **2011**, *72*, 744–748. https://doi.org/10.1016/j.jpcs.2011.03.007

[25] E. Gillet, J. C. Chiarena, M. Gillet, *Surf. Sci.* **1977**, *66*, 613–621. https://doi.org/10.1016/0039-6028(77)90041-3

[26] J. W. Erickson, J. P. Estrup, *Surf. Sci.* **1986**, *167*, 519–533. https://doi.org/10.1016/0039-6028(86)90721-1

[27] P. S. Rao, T. R. Mankhand, P.M. Prasad, *Mat. Trans. JIM* **1996**, *37*, 239–244. https://doi.org/10.2320/matertrans1989.37.239

[28] Y. Hiraoka, K. Imamura, T. Kadokura, Y. Yamamoto, *J. Alloys Com.* **2010**, *489*, 42–46. https://doi.org/10.1016/j.jallcom.2009.09.074

[29] J. I. Imai, O. Taguchi, G. P. Tiwari, Y. Iijima, *Mat. Trans.* **2014**, *55*, 1786–1791. https://doi.org/10.2320/matertrans.M2014277

[30] X. Chen, R. M. de Boer, A. Kosari, H. van Gog, M. A van Huis, *J. Phys. Chem. C* **2023**, *127*, 21387–21398. https://doi.org/10.1021/acs.jpcc.3c05159

[31] Y. Chen, R. Zhang, Z. Hao, Y., Shu, J. He, *Mat. Today Comm.* **2023**, *35*, 105643. https://doi.org/10.1016/j.mtcomm.2023.105643

C. Suryanarayana, *Prog. Mat. Sci.* **2001**, *46*, 1–184. https://doi.org/10.1016/S0079-6425(99)00010-9